

Identification of external influences on temperatures in California

Céline Bonfils · Philip B. Duffy · Benjamin D. Santer ·
Tom M. L. Wigley · David B. Lobell ·
Thomas J. Phillips · Charles Doutriaux

Received: 2 August 2006 / Accepted: 5 October 2007 / Published online: 19 December 2007
© Springer Science + Business Media B.V. 2007

Abstract We use nine different observational datasets to estimate California-average temperature trends during the periods 1950–1999 and 1915–2000. Observed results are compared to trends from a suite of climate model simulations of natural internal climate variability. On the longer (86-year) timescale, increases in annual-mean surface temperature in all observational datasets are consistently distinguishable from climate noise. On the shorter (50-year) timescale, results are sensitive to the choice of observational dataset. For both timescales, the most robust results are large positive trends in mean and maximum daily temperatures in late winter/early spring, as well as increases in minimum daily temperatures from January to September. These trends are inconsistent with model-based estimates of natural internal climate variability, and thus require one or more external forcing agents to be explained. Observational datasets with adjustments for urbanization effects do not yield markedly different results from unadjusted data. Our findings suggest that the warming of Californian winters over the twentieth century is associated with human-induced changes in large-scale atmospheric circulation. We hypothesize that the lack of a detectable increase in summertime maximum temperature arises from a cooling associated with large-scale irrigation. This cooling may have, until now, counteracted summertime warming induced by increasing greenhouse gases effects.

1 Introduction

Human-induced climate change is a reality. Human effects on climate have been identified in many different aspects of the climate system, at global, hemispheric (e.g., Santer et al. 1996; Mitchell et al. 2001; Hegerl et al. 1997; Tett et al. 1999; Stott et al. 2000) and continental

C. Bonfils · P. B. Duffy
University of California, Merced, CA, USA

C. Bonfils (✉) · P. B. Duffy · B. D. Santer · D. B. Lobell · T. J. Phillips · C. Doutriaux
Lawrence Livermore National Laboratory, P.O. Box 808 L-103, Livermore, CA 94550, USA
e-mail: bonfils2@llnl.gov

T. M. L. Wigley
National Center for Atmospheric Research, Boulder, CO, USA

scales (Stott 2003; Zwiers and Zhang 2003; Karoly et al. 2003; Karoly and Braganza 2005). Attempts to detect anthropogenic effects at regional or even grid-point scales are more recent (Spagnoli et al. 2002; Santer et al. 2006; Karoly and Wu 2005). In California, there is great political and scientific interest in the question of how human-caused climate change will manifest itself. Will nighttime temperatures increase more than daytime temperatures? Will there be more warming in winter than in summer? How will precipitation and snow be affected? How uncertain are expected changes? Impacts on agriculture, water availability, human health, etc., depend on answers to these and related questions.

Identification of “fingerprints” of anthropogenic climate change (e.g., due to greenhouse warming or land-use changes) at the scale of the state of California would enhance confidence in model projections of the regional aspects of climate change and their possible societal impacts. Part of such fingerprinting work consists of documenting the background ‘noise’ of natural internal climate variability, and determining whether or not observed trends can be explained by noise alone. The instrumental record is unsuitable for noise estimation because it is too short, and because it is contaminated by the effects of human activities. In model climate change detection work, natural internal variability is estimated from long climate model control simulations with no changes in external factors.

Attribution attempts to identify causal factors responsible for any detected change. Rigorous attribution of observed changes in Californian climate to specific forcings would require “single forcing” experiments, simulating the effects of only one forcing at a time. These are not available from a broad range of climate models. Here, we consider “20CEN” experiments driven by historical changes in combined anthropogenic and natural external forcings, and then determine if these forced simulations yield results consistent with observed changes. Consistency between the observed and 20CEN climate changes, and inconsistency between the observed changes and those from a set of climate model control runs, would imply that we have detected significant changes in Californian climate, and can attribute these changes to the external forcing(s) treated in the simulations. Inconsistencies would point towards errors in (or neglect of) important forcings, and/or errors in the model response to the imposed forcings.

In small domains, detection of externally-forced climate change poses special challenges. Global models are less skillful on sub-continental scales (Stott and Tett 1998), and high-resolution observational datasets are not always available. Furthermore, the noise of internal climate variability generally increases with decreasing domain size, often leading to a degradation of signal-to-noise (S/N) ratios, thus hampering identification of external factors. Finally, forcings that may be of considerable importance in understanding regional climate change (e.g., land-use change, aerosols) are often highly uncertain and spatially and temporally heterogeneous.

We focus on four indices of Californian climate, all of which are based on daily surface air temperatures: monthly-mean temperature (T_{ave}), monthly-mean nighttime minimum and daytime maximum temperatures (T_{min} , T_{max}), and the diurnal temperature range (DTR; $T_{\text{max}} - T_{\text{min}}$). All four indices are well observed in California, and their changes can have important societal impacts. We consider both seasonal and annual mean trends in these indices.

2 Data and methods

Observed California-mean trends in each index are estimated from a minimum of four and a maximum of seven gridded datasets (Table 1), as well as from stations of the US Historical Climatology Network (USHCN and USHCN-U; Karl et al. 1990). Use of multiple datasets

Table 1 Observational data sets, including their spatial and temporal resolution

Acronym	Affiliation	Period ^a	Region	Res	T_{ave}	T_{min}	T_{max}	DTR	Reference
UW1	University Washington	1949–1999	USA	1/8°	Y	Y	Y	Y	Maurer et al. (2002)
UW2	University Washington	1915–2003	West USA	1/8°	Y	Y	Y	Y	Hamlet and Lettenmaier (2005)
UDv1.02	University Delaware	1950–1999	Global	1/2°	Y	–	–	–	Willmott and Matsuura (1998)
NOAA	NOAA NCDC	1851–2000	Global	5°	Y	–	–	–	Eischeid et al. (1995)
HadCRUT2v	Hadley Center	1856–2003	Global	5°	Y	–	–	–	Jones and Moberg (2003)
CRU2.0	University East Anglia	1901–2000	Global	1/2°	Y	Y	Y	Y	Mitchell et al. (2004)
CRU2.1	University East Anglia	1901–2002	Global	1/2°	Y	Y	Y	Y	Mitchell and Jones (2005)
USHCN	Oak Ridge Nat. Lab.	Variable	U.S.	N/A	Y	Y	Y	Y	Karl et al. (1990)

^a In complete years

allows us to assess the robustness of our detection results to observational uncertainty. All datasets (except UW1) are well suitable for long-term trend analysis and include some form of adjustment for non-climatic influences (e.g., changes in instrumentation and station location). The number and coverage of California stations vary between the different observational products. Most datasets are predominantly based on adjusted HCN records. UW1 and UW2 datasets, however, have higher station coverage over California, and include both HCN and Cooperative network observations. The CRU2.0, CRU2.1, UW1 and USHCN datasets were not adjusted for urbanization effects, while the HadCRUT2v, UW2 and USHCN-U datasets attempt to account for urbanization. None of the observational datasets accounts for the effects of other human-induced changes in land-surface properties, such as conversion to crop-land, irrigation, etc.

Although the datasets analyzed here rely on similar raw data and are not completely independent, the processing choices made by dataset developers can differ markedly from group to group, leading to uncertainty in the magnitude (and sometimes even the sign) of the observed trends (see Figs. 1 and 2). Here, the main period of interest is 1950–1999,

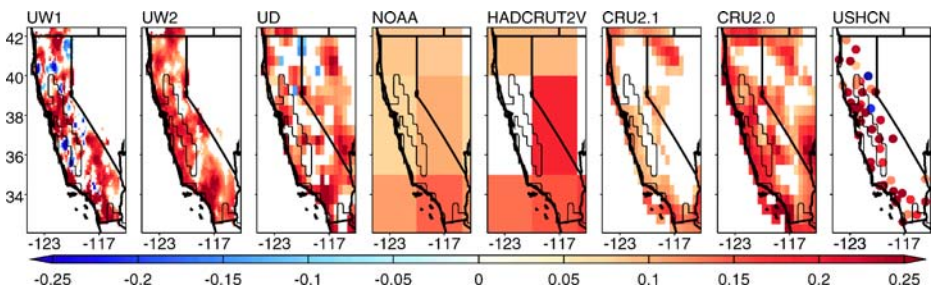


Fig. 1 Spatial patterns of annual-mean temperature trends (°C/decade) in different observational datasets. At each grid-cell, trends were estimated by a least-squares linear fit to times series of temperature anomalies over 1950–1999. Trends that are not statistically different from zero at the 80% confidence level are in white. The 150-m contour roughly delineates California’s Central Valley

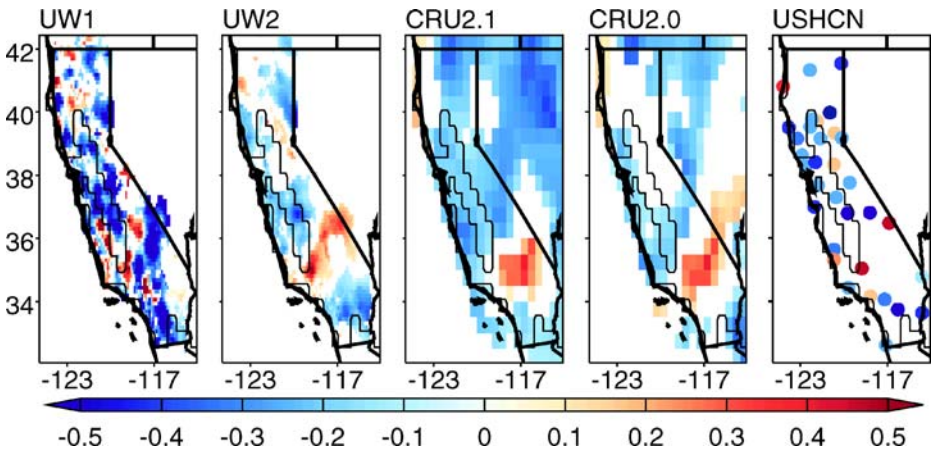


Fig. 2 As for Fig. 1, but for trends in diurnal temperature range

because it contains the most reliable historical records and is covered by all datasets. However, we also examine temperature changes over 1915–2000, the longest period covered by most datasets.

In Section 3, we investigate whether observed historical trends in California exceed climate ‘noise’ by comparing observed trends in T_{ave} , T_{min} , T_{max} , and DTR to distributions of modeled linear trends from unforced control simulations (this approach has been used by Karoly et al. 2003; Santer et al. 2006). For this purpose, we used 22 (for T_{ave}) or 6 (for T_{min} , T_{max} , and DTR) long control simulations. After establishing that some observed trends are inconsistent with results of unforced simulations, we compare the observed T_{ave} (T_{min} , T_{max} , and DTR) trends to those from 69 (15) 20CEN historical runs performed with 22 (8) different models. The 20CEN runs are forced by combinations of external factors (greenhouse gases, sulfate aerosols, volcanic aerosols, solar irradiance...) that are model-dependent (Table 2). All simulation were performed in support of the IPCC Fourth Assessment Report (AR4).

In order to create distributions of model-derived unforced trends, linear trends were fitted, for each control simulation, to overlapping 50- or 86-year segments (separated by 10-year intervals) of the California-average temperature time series. These multi-model distributions reflect noise uncertainties arising from differences in a wide range of model properties (physics, parameterizations, resolution, etc.), and provide the best available model-based estimates of natural internal variability.

The significance of observed trends was assessed in two ways: (1) by comparing observed trends with the 95% confidence intervals of the unforced trend distributions, computed by assuming a Gaussian distribution of trends and multiplying the standard error of the distribution (s_E) by 1.96; (2) by determining the empirical probability that the magnitude of the unforced trends exceeds that of observed trends. The two methods give very similar results, supporting the assumption of the Gaussian distribution of trends (Fig. 3). While none of the control runs has a statistically significant overall temperature trend for the Californian domain, some simulations do show residual drift at the beginning of the run (Santer et al. 2006). Additionally, one shows a sudden jump that seems pathological. We opted to retain the trends arising from these initial drifts and jump, thus inflating s_E and making it more difficult to reject the null hypothesis that an observed trend is due to natural internal variability.

Table 2 Characteristics of climate simulations

Model designation	Resolution	Originating group (s)	R_a	R_b	Forcings	Y_1	Y_N	L	N_a	N_b
CCSM3	T85	NCAR, USA	6	2	ABCFJK	280	509	230	19	–
GFDL-CM2.0	2.0×2.5°	GFDL, USA	3	–	ABCFJK	1	500	500	46	–
GFDL-CM2.1	2.0×2.5°	GFDL, USA	3	–	ABCFJK	1	500	500	46	–
GISS-EH	4.0×5.0°	GISS, USA	5	–	ABCDEFHIJK	1,880	2,279	400	36	–
GISS-ER	4.0×5.0°	GISS, USA	9	–	ABCDEFHIJK	1,901	2,400	500	46	–
MIROC3.2(medres)	T42	CCSR/NIES/FRCGC, Japan	3	3	ABCFJK	2,300	2,799	500	46	46
MIROC3.2(hires)	T106	CCSR/NIES/FRCGC, Japan	1	1	ABCDEFHIJK	1	100	100	6	6
MIUB/ECHO-G	T30	MIUB/METRI/MD Germ./Korea	5	–	ACDIJK	1860	2200	341	30	–
MRI-CGCM2.3.2	T42	MRI, Japan	5	–	ACIK	1,851	2,200	350	31	–
PCM	T42	NCAR, USA	4	2	ABCJK	451	1,079	629	58	–
UKMO-HadGEM1	1.25×1.87°	UKMO, UK	2	–	ABCDEFJK	1,927	2,098	172	13	–
BCCR-BCM2.0	T63	BCCR, Norway	1	1	AC	1,850	2,099	250	21	21
CCCma-CGCM3.1(T47)	T47	CCCma, Canada	5	–	AC	1,850	2,850	1001	96	–
CCCma-CGCM3.1(T63)	T63	CCCma, Canada	1	–	AC	1,850	2,199	350	31	–
CNRM-CM3	T63	CNRM, France	1	–	ABCE	1,930	2,429	500	46	–
CSIRO-Mk3.0	T63	CSIRO, Australia	3	3	AC	1,871	2,250	380	34	34
ECHAM5/MP1-OM	T63	MPI, Germany	3	–	ABCD	2,150	2,655	506	46	–
FGOALS-g1.0	T42	LASG/IAP, China	3	–	AC	1,850	2,199	350	31	–
GISS-AOM	3.0×4.0°	GISS, USA	2	2	ACH	1,850	2,100	251	21	21
INM-CM3.0	4.0×5.0°	INM, Russia	1	1	ACJ	1,871	2,200	330	29	9
IPSL-CM4	2.5×3.75°	IPSL, France	1	–	ACD	1,860	2,359	500	46	–
UKMO-HadCM3	2.5×3.75°	UKMO, UK	2	–	ABCD	1,859	2,200	342	30	–
TOTAL	–	–	69	15	–	–	–	–	808	137

See PCMDI web site (<http://www-pcmdi.llnl.gov> for more details)

R_a , R_b Number of twentieth century climate realizations available for T_{ave} and for T_{min} , T_{max} ; forcings used in the twentieth century runs (Santer et al. 2006): A Greenhouse gases, B Ozone, C sulfate aerosol direct effects, D sulfate aerosol indirect effects, E black carbon, F organic carbon, G mineral dust, H sea salt, I land-use change, J Solar irradiance, K volcanic aerosols; Y_1 , Y_N , L model-specific choices for the starting year, the ending year, and the length (in years) of the control runs; N_a , N_b number of overlapping 50-year linear trends obtained from each control run for T_{ave} and for T_{min} , T_{max} ; DTR (when data are supplied)

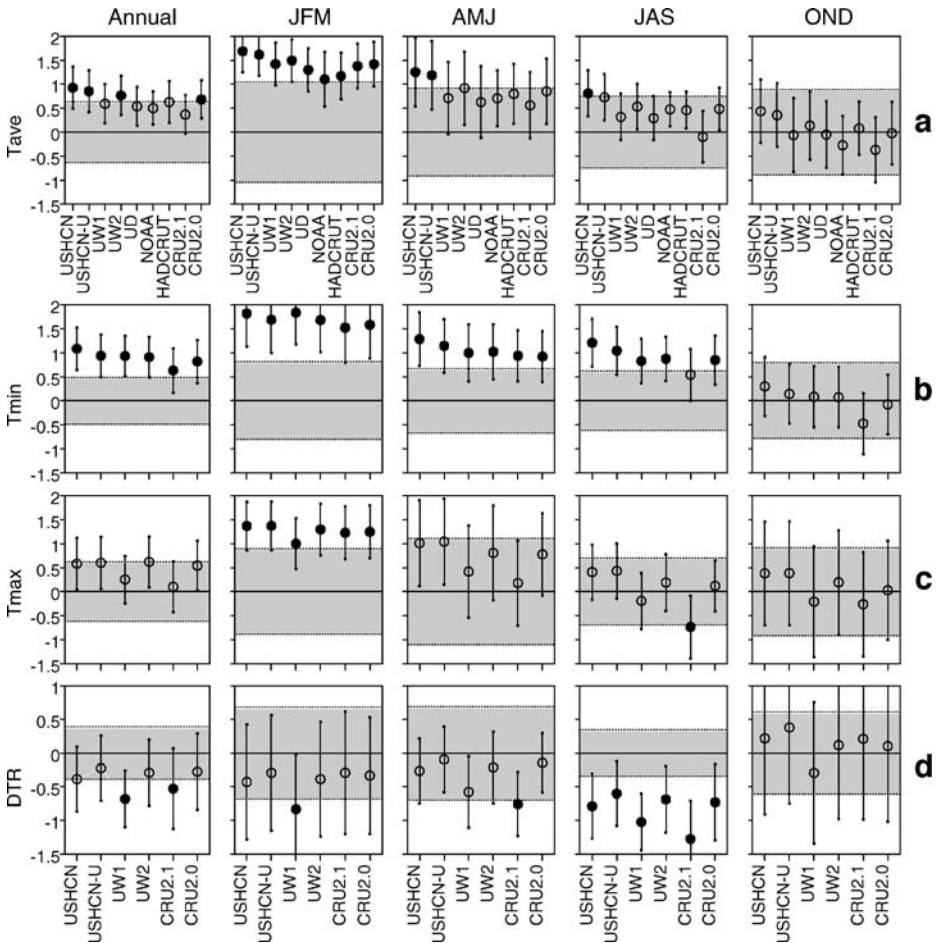


Fig. 3 Observed temperature trends over 1950–1999 (circles) and model-derived estimates of natural internal variability (in deg C/50 years). Climate noise estimates are based on multi-model unforced 50-year trend distributions (see main text). The upper and lower limits of the shaded area represent the 95% confidence intervals of the trend distributions and were computed as $\pm 1.96 \times s_E$, the standard error of the sampling distribution. Results are for **a** daily-mean temperature; **b** daily minimum temperature; **c** daily maximum temperature; **d** diurnal temperature range. Vertical bars represent the standard error for the trend (accounting for the temporal autocorrelation of the regression residuals) $\times 1.641$ (one-tailed *t* test, 5% level; see Santer et al. 2000). Circles are filled when the empirical probability for the magnitude of the unforced trends to exceed that of observed trends is less than 5%. Data from different USHCN stations are equally weighted

The detection procedure outlined above was applied to annual- and seasonal-mean [January–March (JFM), April–June (AMJ), July–September (JAS), and October–December (OND)] values of the four indices considered here. We used this somewhat unconventional seasonal definition because observed trends in December are very different from those in January (see below).

The reliability of the detection results depends crucially on the fidelity with which the models used here simulate the natural internal variability of the real-world climate system. This is difficult to assess, particularly on the multi-decadal timescales of interest here, without multi-century observational records uncontaminated by human influences.

However, observational data are of adequate length to make meaningful comparisons of modeled and observed temperature variability on annual and decadal timescales (e.g. Stott 2003; Braganza et al. 2004; Santer et al. 2006). Accurate simulation of natural variability on these shorter timescales would enhance our confidence in the detection of externally-forced multi-decadal trends. We compared the observed interannual and decadal variability of each temperature index with corresponding values from the 20CEN realizations. The (varying) length of the observational record dictated the period used for calculating model and observed temporal standard deviations. All standard deviations were computed after first removing the overall linear trend from the area-average data, which constitutes a zero-order estimate of the influence of external forcing. The interannual variability is simply the standard deviation of the residuals. The decadal standard deviation is computed after low-pass filtering the regression residuals with a Lynch and Huang (1992) digital filter with half-power at a period of 119 months (Santer et al. 2006). The results of this variability comparison are discussed in Section 4.

3 Results of detection analysis

All gridded observational datasets show a consistent pattern of increasing annual-mean temperatures and decreasing annual-mean DTR over the period 1950–1999. Over most of California, these observed trends are different from zero with a high degree of statistical significance (Figs. 1 and 2). Similar results are found for the USHCN station data. Such consistency across multiple datasets increases our confidence in the reality of the annual-mean T_{ave} and DTR changes. Annual-mean T_{ave} increased by 0.36 to 0.92°C over 1950–1999, depending on the observational dataset considered. Using the distribution of the unforced trends, four of the nine observed trends (for USHCN, USHCN-U, UW2, and CRU2.0) are significantly different from the model-derived internal climate variability at the 5% confidence level or better (Fig. 3). T_{ave} changes are largest in wintertime and exceed model-derived noise estimates in all nine observational datasets. This strongly suggests that external forcing(s) are required to explain the observed JFM trends in T_{ave} . Two datasets (USHCN and UW2) have significant T_{ave} trends in spring. No observational dataset yields significant T_{ave} trends in summer or fall.

This analysis of daily-mean temperatures masks interesting information contained in the diurnal cycle of temperature change. Substantial nighttime warming occurs in every month except December (not shown), and trends in T_{min} are inconsistent with internally-generated climate noise in every season except OND (Fig. 3b). In contrast, monthly trends in observed daily maximum temperatures exceed estimated internal variability only in late winter/early spring (Fig. 3c), with largest warming of T_{max} in January and March (1.5°C over 50 years), reduced warming in February (0.5°C over 50 years) and cooling in December. Observed trends in DTR exceed the estimated noise during summer only (Fig. 3d), reflecting the much greater increase in minimum temperature than in maximum temperature in those months. Although the amplitude of nighttime warming is smaller in USHCN-U than in USHCN dataset, the detection results are not sensitive to the inclusion of adjustments for urbanization effects (compare USHCN vs USHCN-U, CRU2.0 and CRU2.1 vs HadCRUT2v, and UW1 vs UW2).

Californian temperature changes over 1915–2000 are even more difficult to explain by internal climate noise alone (Fig. 4). In all but one dataset, the estimated increase in annual-mean T_{ave} is significant at the 5% level. Positive detection is not limited to the winter season, but extends to the spring and summer seasons for most observational datasets.

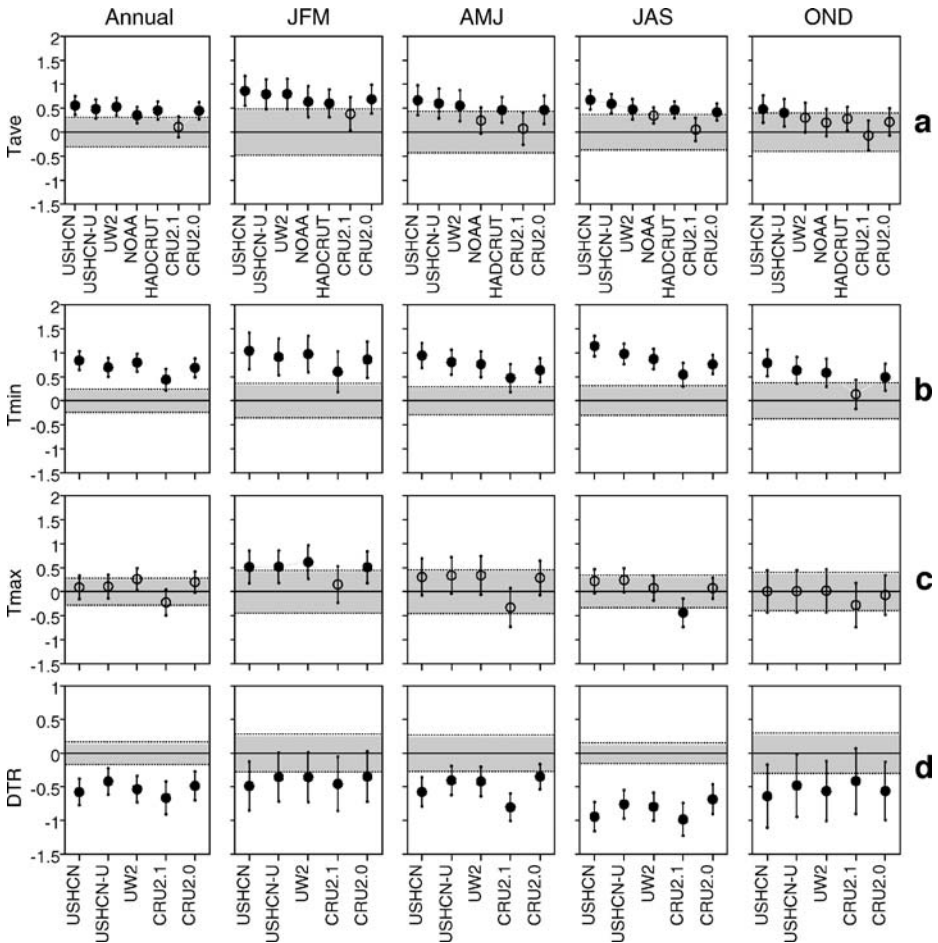


Fig. 4 Same as Fig. 3, but observed trends are computed over the period 1915–2000, and the range of natural internal variability is based on multi-model unforced 86-year trend distributions

Similarly, trends in T_{\min} and DTR are inconsistent with internally-generated climate noise during all seasons. Again, those results are not sensitive to the inclusion or exclusion of urbanization adjustments. Enhanced detectability at longer timescales is an expected characteristic of a slowly-evolving greenhouse-gas signal, as is evident in Santer et al. (1996, 2006).

We consider next whether observed changes in Californian temperature indices are consistent with results from the forced 20CEN model simulations with combined anthropogenic and natural forcings (Table 2). In general, the models fail to reproduce the observed seasonality of changes in T_{ave} , T_{\min} , T_{max} , and DTR (Fig. 5, lower panels). While most simulations capture the observed JAS trends in T_{ave} and T_{\min} (but not T_{max} and DTR), they tend to underestimate the observed JFM trends in T_{ave} , T_{\min} , and T_{max} .

Such deficiencies in the simulation of regional trends are not surprising, and have a number of possible explanations. First, many of the 20CEN runs examined here do not incorporate changes in spatially- and temporally heterogeneous forcings (such as land-use, carbonaceous aerosols, indirect aerosol effects, etc., Santer et al. 2006). Because these

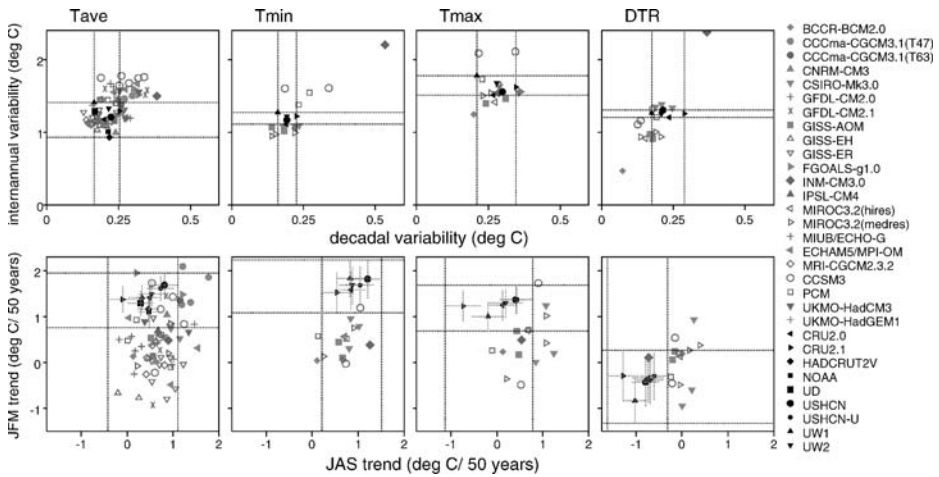


Fig. 5 Comparison of statistical properties of four simulated and observed temperature indices in California. Simulations are forced 20CEN historical runs. *Upper panels* Standard deviations of filtered and unfiltered detrended observed and control model time-series for the period 1915–1999 (except for UW2, UW1 and UD, see text). *Lower panels* 1950–1999 trends in summer (*JAS*) and winter (*JFM*). Observational data sets are in *black* and include a 1σ trend confidence interval adjusted for temporal autocorrelation effects. Individual realizations from 22 global climate models are in *grey*. *Vertical and horizontal lines* denote the minimum and maximum observed values, and facilitate comparison with model results

forcings have probably made significant contributions to regional-scale climate change, we do not expect the historical simulations to perfectly match the data. Second, even models that include some representation of heterogeneous and highly uncertain forcings may lack the spatial resolution to reliably represent the climate response to the imposed forcings: the entire state of California is represented by a minimum of 5 and maximum of 35 grid-boxes in the AR4 models analyzed here. Third, comparison of multiple 20CEN realizations performed with the same model reveal that individual realizations can have very different 50-year trends. Reliable estimation of the true response to the imposed forcing changes may require larger ensemble sizes than were available in the IPCC AR4 database (Table 2). Finally, the model- vs observed differences may reflect real model errors, both at large scales and at regional scales.

4 Discussion

Karoly et al. (2003) have performed a similar detection analysis, focusing on land surface temperature changes over North America (between 30N° and 65°N). They found that the increase in annual-mean surface air temperature from 1950 to 1999 and from 1900 to 1999 (in HadCRUT2v) could not be explained by natural internal variability. Our results for Californian temperature changes over the last 50- and 86 years are broadly consistent with Karoly et al.’s findings. However, while Karoly et al. reported an observed DTR decrease that was indistinguishable from control run noise over 1950–1999, but distinctly different from unforced variability over the period 1900–1999, we obtained significant annual-mean DTR decreases at both timescales in some observational datasets.

Our conclusion that external factors are perturbing the climate in California depends on the reliability of the model-based noise estimates. As discussed above, it is not possible to evaluate the model noise simulations on the multi-decadal timescales that are most relevant

to the detection issues addressed here. However, observational data are of adequate length to test model simulations of interannual and decadal-timescale noise. Our confidence in the trend significance results presented here would be diminished if the models systematically underestimated noise on these shorter timescales. There is no evidence that this is the case (Fig. 5, top panels).

For T_{ave} , Stott and Tett (1998) found that an earlier version of the Hadley Centre models used here (HADCM2) generally underestimated climate variability at spatial scales below 2000 km. Our T_{ave} results for California indicate that none of the AR4 models has interannual variability below the lower end of the range of observational estimates, and only two models (GISS-ER and MRI-CGCM2.3.2) systematically underestimate the decadal variability (i.e., each of their 20CEN realizations lies below the observational range). The fact that most AR4 models do not underestimate decadal variability increases confidence in our model-based estimates of longer-timescale climate noise, but does not rule out systematic errors in those estimates. For T_{min} , T_{max} , and DTR indices, fewer observational datasets and simulations are available. None of the models examined here systematically underestimates the magnitude of decadal variability for either T_{min} or T_{max} . For DTR, however, interannual and decadal variability is systematically underestimated by CCSM3, INM-CM3.0 and MIROC3.2(hires), suggesting that their covariability between T_{min} and T_{max} is too high, while these indices are more decoupled in other models and in observations.

In the following section, we attempt to understand the pronounced seasonality of observed temperature trends in California. Christy et al. (2006), using their own observational temperature dataset, reported rapid nighttime warming in the Central Valley over 1910 to 2003, but not in surrounding mountains. They attribute this warming to the effects of large-scale irrigation (an interpretation questioned by Bonfils et al. 2006), but do not identify the physical mechanism responsible for the change. Bereket et al. (2005) attribute nighttime warming in the Valley to increased population, urbanization, and road construction. None of these mechanisms, however, explains the pronounced seasonal variations in temperature trends.

In JFM, observed trends in T_{min} , T_{max} and T_{ave} are unlikely to be explained by natural internal variability alone. A larger JFM warming trend is consistent with a stronger snow-albedo feedback in this season, but the spatial pattern of the observed warming does not clearly support this interpretation. A more plausible explanation is that a trend towards warmer California winters is associated with a long-term change in large-scale atmospheric circulation over the North Pacific Ocean. This change is characterized by a southward shift of wind fields over the central North Pacific and a northward shift over the west coast of North America (Dettinger and Cayan 1994, their Fig. 10d). Analysis of trends in NCEP-50 observed JAS 700 mb height anomalies reveals that the circulation-change patterns identified by Dettinger and Cayan are very pronounced in January and March (months characterized by robust detection in trends of T_{min} , T_{max} and T_{ave}), with a concurrent warming in coastal sea surface temperatures. This circulation change is less pronounced in February and is qualitatively different in December, consistent with observed temperature trends.

The results of other studies suggest that greenhouse-gas forcing is likely to be involved in this seasonal circulation shift. First, Zwiers and Zhang (2003) found that the combined effects of greenhouse gas and sulfate aerosol forcing caused significant North American warming in wintertime only. Second, Shindell et al. (2001) linked increasing greenhouse gas concentrations with increased flow of warm air from the Pacific Ocean to western North America, consistent with Dettinger and Cayan's analysis. Finally, Gillett et al. (2005) detected an anthropogenic signal in DJF sea-level pressure trends over 1948–1998, with a

coherent decrease over the North Pacific and an increase over the west coast of North America, features that coincide with those noted by Dettinger and Cayan. Gillett et al. also found that models underestimate this circulation change, which may explain why the rise in JFM T_{ave} in the AR4 simulations is weaker than in observations (Fig. 5, lower panel).

In summer, the externally-forced trend towards warmer nights is captured by at least one realization of every model (except for the single realization of BCCR-BCM2.0). However, most models overestimate daytime warming (which is weak in the observations, and not distinguishable from noise). Consequently, significant summertime changes in DTR are not reproduced by the models. One interpretation of this result is that the 20CEN simulations neglect an important regional forcing. An obvious candidate is irrigation, which is widely employed in California, and is not represented in 20CEN simulations performed with global models. Although the effect of irrigation on nighttime temperature remains somewhat uncertain, irrigation causes daytime evaporative cooling (Lobell et al. 2006; Kueppers et al. 2007). At the global scale, the much smaller annual-mean increase in T_{max} than in T_{min} (Karl et al. 1993) is not captured by global models. This may be due to either an absence of a significant cloudiness trend that is present in observations (Braganza et al. 2004) or to the lack of prognostic photosynthesis in most global models (Bonfils et al. 2004). In the Central Valley, summertime cloudiness is probably too low to be implicated in explaining differential T_{min} and T_{max} trends. Irrigation is a more credible hypothesis, and appears consistent with the observed cooling of summer days and warming of summer nights in the Central Valley, and day- and nighttime warming elsewhere.

In summary, the JAS trends in Fig. 3 can be interpreted in several ways. One explanation is that trends in T_{max} over California are due to natural climate fluctuations alone. A more plausible interpretation (in view of the large temporal changes in irrigation in the Central Valley, the likely physical impacts of these changes, and their absence in 20CEN simulations) is that irrigation-induced cooling of T_{max} has obscured a warming signal arising from the combined effects of greenhouse gases and urbanization.

5 Conclusions

We show that external forcing(s) are perturbing the climate of California. The domain size is smaller than that used in most previous regional-scale detection studies. However, by employing multiple observational and model datasets, we gained confidence in both the robustness of the observed signals and their detection relative to model noise estimates. We hypothesize that the rise in late winter/early spring temperatures (T_{ave} , T_{min} , T_{max}) is associated with long-term changes in large-scale atmospheric circulation that are human-induced. It is also likely that the lack of a significant T_{max} trend in summer reflects a partial offsetting of the greenhouse-gas-induced warming by an evaporative cooling occurring in irrigated regions. More work is needed to solidify these findings.

One implication of our findings is that anthropogenic forcings may be more readily detectable in regional-scale ocean surface temperature changes (Santer et al. 2006), than in regional-scale land-surface temperature changes. The latter are more strongly influenced by local factors, such as changes in land-use (e.g. irrigation, urbanization) and anthropogenic aerosols, which are difficult to simulate accurately. High-resolution, multi-decadal transient simulations of the effects of individual forcings would be very helpful in regional detection and attribution work. Such simulations have not been performed to date, in part due to computational limitations, and in part because reliable information on the forcings themselves is not always available (e.g., detailed descriptions of historical changes in land-use patterns).

Finally, in the case of forcings such as aerosols, there are still significant uncertainties in both our understanding of their climatic effects and our ability to correctly model these effects. Nevertheless, our study represents a credible first step towards the identification and physical interpretation of the effects of external forcings on Californian climate.

Acknowledgments This work was supported by the State of California through the Public Interest Energy Research Program. We acknowledge the modeling groups for providing data for analysis, and PCMDI for collecting and archiving the model data. The IPCC Data Archive at Lawrence Livermore National Laboratory is supported by the Office of Science, U.S. Department of Energy. The USHCN dataset was developed and is maintained at the National Climatic Data Center (NCDC) and the Carbon Dioxide Information and Analysis Center (CDIAC) of Oak Ridge National Laboratory. NCEP Reanalysis and UD data were provided by the NOAA-CIRES Climate Diagnostics Center, Boulder, Colorado, USA, via their web site <http://www.cdc.noaa.gov/>. HadCRUT2v, CRU2.0 and CRU2.1 were provided by the Climatic Research Unit (<http://www.cru.uea.ac.uk/cru/data/>). The NOAA (National Oceanic and Atmospheric Administration) dataset was produced by the Global Climate Perspectives System (GCPS) and obtained from the NCDC. UW1 and UW2 meteorological data were obtained from the Surface Water Modeling group at the University of Washington via the web site at http://www.hydro.washington.edu/Lettenmaier/gridded_data. We thank Alan Hamlet (University of Washington), Edwin Maurer (Santa Clara University) and Phil Jones (Climatic Research Unit) for providing information regarding their datasets.

References

- Bereket L, Fabris D, Gonzalez JE, Chiappari S, Zarantonello S, Miller NL, Bornstein R (2005) Urban heat islands in California's Central Valley. *Bull Am Meteorol Soc* 86:1542–1543
- Bonfils C, Duffy PB, Lobell DB (2006) Comment on 'Methodology and results of calculating Central California surface temperature trends: evidence of a human-induced climate change?'. *J Clim* 20:4486–4489
- Bonfils C, Fung I, Doney S, John J (2004) On the detection of summertime terrestrial photosynthetic variability from its atmospheric signature. *Geophys Res Lett* 31:L09207
- Braganza K, Karoly DJ, Arblaster JM (2004) Diurnal temperature range as an index of global climate change during the twentieth century. *Geophys Res Lett* 31:L13217
- Christy JR, Norris WB, Redmond K, Gallo KP (2006) Methodology and results of calculating Central California surface temperature trends: evidence of a human-induced climate change? *J Clim* 19:548–563
- Dettinger MD, Cayan DR (1994) Large-scale atmospheric forcing of recent trends toward early snowmelt runoff in California. *J Clim* 8:606–623
- Eischeid JK, Baker CB, Karl TR, Diaz HF (1995) The quality control of long-term climatological data using objective data analysis. *J Appl Meteor* 34:2787–2795
- Gillett NP, Allan RJ, Ansell TJ (2005) Detection of external influence on sea level pressure with a multi-model ensemble. *Geophys Res Lett* 32:L19714
- Hamlet AF, Lettenmaier DP (2005) Production of temporally consistent gridded precipitation and temperature fields for the continental U.S. *J Hydrometeorology* 6:330–336
- Hegerl GC, Hasselmann K, Cubasch U, Mitchell JFB, Roeckner E, Voss R, Waszkewitz J (1997) Multi-fingerprint detection and attribution analysis of greenhouse gas, greenhouse gas-plus-aerosol and solar forced climate change. *Clim Dyn* 13:613–634
- Jones PD, Moberg A (2003) Hemispheric and large-scale surface air temperature variations: An extensive revision and an update to 2001. *J Clim* 16:206–223
- Karl TR, Jones PD, Knight RW, Kukla G, Plummer N, Razuvayev V, Gallo KP, Lindesay J, Charlson RJ, Peterson TC (1993) A new perspective on recent global warming—Asymmetric trends of daily maximum and minimum temperatures. *Bull Amer Meteor Soc* 74:1007–1023
- Karl TR, Williams CN Jr, Quinlan FT (1990) U.S. Historical Climatology Network (HCN) Serial Temperature and Precipitation Data. ORNL/CDIAC-30, NDP-019/R1. Carbon Dioxide Information Analysis Center, Oak Ridge National Laboratory, U.S. Department of Energy, Oak Ridge, Tennessee
- Karoly DJ, Braganza K (2005) A new approach to detection of anthropogenic temperature changes in the Australian region. *Meteorol Atmos Phys* 89:57–67
- Karoly DJ, Wu Q (2005) Detection of regional surface temperature trends. *J Clim* 18:4337–4343
- Karoly DJ, Braganza K, Stott PA, Arblaster JM, Meehl GA, Broccoli AJ, Dixon KW (2003) Detection of a human influence on North American climate. *Science* 302:1200–1203

- Kueppers LM, Snyder MA, Sloan LC, Cayan D, Jin J, Kanamaru H, Kanamitsu M, Miller NL, Tyree M, Du H, Weare B (2007) Seasonal temperature responses to land-use change in the western United States. *Glob Planet Change* (in press)
- Lobell D, Bala G, Duffy PB (2006) Biogeophysical impacts of cropland management on climate. *Geophys Res Lett* 33:L06708
- Lynch P, Huang X-Y (1992) Initialization of the Hirlam model using a digital-filter. *Mon Weath Rev* 120:1019–1034
- Maurer EP, Wood AW, Adam JC, Lettenmaier DP, Nijssen B (2002) A long-term hydrologically-based data set of land surface fluxes and states for the conterminous United States. *J Clim* 15:3237–3251
- Mitchell JFB, Karoly DJ, Hegerl GC, Zwiers FW, Allen MR, Marengo J (2001) Detection of climate change and attribution of causes. In: Houghton JT et al. (eds) *Climate Change 2001: The Scientific Basis, Contribution of Working Group I to the Third Assessment Report of the Intergovernmental Panel on Climate Change*. Cambridge University Press, Cambridge, pp. 695–738
- Mitchell TD, Carter TR, Jones PD, Hulme M, New M (2004) A comprehensive set of high-resolution grids of monthly climate for Europe and the globe: the observed record (1901–2000) and 16 scenarios (2001–2100). Tyndall Working Paper 55, Tyndall Centre, UEA, Norwich. UK. <http://www.tyndall.ac.uk/>
- Mitchell TD, Jones PD (2005) An improved method of constructing a database of monthly climate observations and associated high-resolution grids. *Int J Climatol* 25:693–712
- Santer BD, Taylor KE, Wigley TML, Johns TC, Jones PD, Karoly DJ, Mitchell JFB, Oort AH, Penner JE, Ramaswamy V, Schwarzkopf MD, Stouffer RJ, Tett S (1996) A search for human influences on the thermal structure of the atmosphere. *Nature* 382:39–46
- Santer BD, Wigley TML, Boyle JS, Gaffen DJ, Hnilo JJ, Nychka D, Parker DE, Taylor KE (2000) Statistical significance of trends and trend differences in layer-average atmospheric temperature time series. *J Geophys Res* 105:7337–7356
- Santer BD, Wigley TML, Gleckler PJ, Bonfils C, Wehner MF, AchutaRao K, Barnett TP, Boyle JS, Bruggemann W, Fiorino M, Gillett N, Hansen JE, Jones PD, Klein SA, Meehl GA, Raper SCB, Reynolds RW, Taylor KE, Washington WM (2006) Causes of ocean surface temperature changes in Atlantic and Pacific hurricane formation regions. *Proc Natl Acad Sci U S A* 103:13905–13910
- Shindell DT, Schmidt GA, Miller RL, Rind D (2001) Northern Hemisphere winter climate response to greenhouse gas, ozone, solar, and volcanic forcing. *J Geophys Res* 106:7193–7210
- Spagnoli B, Planton S, Deque M, Mestre O, Moisselin J-M (2002) Detecting climate change at a regional scale: the case of France. *Geophys Res Lett* 29:1450
- Stott PA (2003) Attribution of regional-scale temperature changes to anthropogenic and natural causes. *Geophys Res Lett* 30:1728
- Stott PA, Tett SFB (1998) Scale-Dependent Detection of Climate Change. *J Clim* 11:3282–3294
- Stott PA, Tett SFB, Jones GS, Allen MR, Mitchell JFB, Jenkins GJ (2000) External control of 20th century temperature by natural and anthropogenic forcings. *Science* 290:2133–2137
- Tett SFB, Stott PA, Allen MR, Ingram WJ, Mitchell JFB (1999) Causes of twentieth-century temperature change near the Earth's surface. *Nature* 399:569–572
- Willmott CJ, Matsuura K (1998) *Global air temperature and precipitation: regridded monthly and annual climatologies (version 2.01)*, Newark, Delaware: Center for Climatic Research. Dept. of Geography, Univ. of Delaware
- Zwiers FW, Zhang X (2003) Towards regional climate change detection. *J Clim* 16:793–797